arXiv:astro-ph/9801084v1 12 Jan 1998

Inward Propagation of Nuclear-Burning Shells in Merging C-O and He White Dwarfs

Hideyuki Saio

Astronomical Institute, School of Science, Tohoku University, Sendai 980, Japan ; saio@astr.tohoku.ac.jp

and

Ken'ichi Nomoto

Department of Astronomy & Research Center for the Early Universe, School of Science, University of Tokyo, Bunkyo-ku, 113, Japan, and Institute for Theoretical Physics, the University of California at Santa Barbara, CA; nomoto@astron.s.u-tokyo.ac.jp

ABSTRACT

We have investigated the consequences of merging double white dwarf systems by calculating evolutionary models of accreting white dwarfs. We have considered two cases; a massive C-O white dwarf of $\sim 1M_\odot$ accreting C-O mixture, and a low mass white dwarf with an initial mass of $0.4M_\odot$ accreting matter composed mostly of helium.

The accretion rate of the C-O white dwarf is assumed to be $1 \times 10^{-5} M_\odot \mathrm{y}^{-1}$. After carbon burning is ignited at $M_r \sim 1.04M_\odot$, the flame propagates inward due to heat conduction. By inserting enough grid points to resolve the structure of the flame, we have obtained almost steady burning in most phase of evolution, but we have found a new phenomenon that the strength of flame sometimes oscillates due to a *thermal instability* in early phase of the evolution. In calculating evolutionary models, we have occasionally employed a steady-burning approximation, in which the propagation speed of flame is given a priori. We have considered two extreme cases for the interior abundance of the massive white dwarf: $X_\mathrm{C} = 0.5$ and $X_\mathrm{C} = 0.2$. For $X_\mathrm{C} = 0.5$, the flame becomes very weak at $M_r \sim 0.4M_\odot$ and the inward propagation stall there. But a few thousand years later, the flame is reactivated due to contraction and propagates to the center. For $X_\mathrm{C} = 0.2$, the flame propagates smoothly and reaches the center in ~ 1000 years. In both cases the C-O mixture has been burned into an O-Ne-Mg mixture without causing an explosive phenomenon.

For helium accreting low mass white dwarfs, we have considered accretion rates of 1×10^{-7} and $1 \times 10^{-6} M_\odot \mathrm{y}^{-1}$. After a fraction of $M_\odot$ is accreted to the white dwarf, helium is ignited in the outer part and a shell flash occurs. Such a shell flash diminishes when about 10% of helium in the convective shell is burned into carbon and oxygen. The next shell flash occurs at a shell interior to the previously flashed shell. After less than 30 shell flashes, the helium ignition occurs at the center and steady burning begins. Thus, the merging produces a helium star which burns helium at the center. The mechanism of the propagation of the burning shell in this case is compressional

heating during inter-pulse phases, in contrast to the case of carbon-burning flame where the conduction drives the inward propagation of the flame. We infer that such a low mass double white dwarf system could be a progenitor of the AM CVn stars.

Subject headings: stars: evolution – stars: white dwarfs – stars: binary – stars: chemically peculiar – stars: supernova

1. Introduction

It is expected theoretically that a fraction of close binary systems become double white dwarf systems (Iben & Tutukov 1984; Webbink 1984). Observationary, several double white dwarf systems have been found by Nather, Robinson, & Stover (1981), Saffer, Liebert, & Olszewski (1988), Bragaglia, et al. (1990), Marsh, Dhillon, & Duck (1995), and Marsh (1995). Although low mass white dwarfs ($M < 0.45 M_\odot$) are often found in binary systems (Marsh et al. 1995), no massive double white dwarf system with a short period (less than several hours) has been found despite several searches by e.g., Robinson & Shafter (1987), Foss, Wade & Green (1991), and Bragaglia et al. (1990). Bragaglia (1995) discussed the present status of the search and possible explanations for the null result. In this paper, we assume that there exist some massive double white dwarf systems as well as low mass systems.

Double white dwarf systems having short enough periods are expected to merge within the Hubble time by the effect of gravitational wave radiation. Since the radius of a white dwarf is proportional to $M^{-1/3}$, once the less massive component fills its critical Roche lobe, a dynamical mass transfer occurs if the secondary to primary mass ratio is sufficiently large (Cameron & Iben 1986; Benz et al. 1990). The consequence of the rapid mass transfer seems to be the formation of a hot thick disk around the primary white dwarf (e.g., Hachisu, Eriguchi, & Nomoto 1986; Mochkovich & Livio 1990). At least a part of the disk matter eventually falls on the white dwarf to complete the merging process. Iben & Tutukov (1984) and Webbink (1984) argued that if the total mass of the two white dwarfs is larger than Chandrasekhar's limiting mass, the merging would lead to a Type Ia supernova. Whether it occurs or not, however, depends on the accretion rate onto the white dwarf, which, in turn, depends on the timescale on which the angular momentum distribution changes significantly in the thick disk. As discussed by Mochkovich & Livio (1990), the timescale can be as short as a few days if the thick disk is turbulent. In such a case, the accretion onto the white dwarf is limited by the Eddington limit ($\dot{M} \sim 2 \times 10^{-5} M_\odot \mathrm{y}^{-1}$ for $M \sim 1 M_\odot$) due to the effect of radiation pressure. For such a high accretion rate, Nomoto & Iben (1985) have shown that carbon-burning is ignited in an outer shell of the white dwarf due to the effect of compressional heating. Saio & Nomoto (1985) and Woosley & Weaver (1986) have shown that carbon-burning ignited near the surface propagates to the center to burn most of carbon without causing an explosive phenomenon. In these calculations the propagation of carbon-burning was simulated as successive phases of a shell-flash and an inter shell-flash, because the burning region (flame) was not spatially resolved.

To overcome the poor resolution in stellar evolution models, Timmes, Woosley, & Taam (1994) calculated the propagation of flame in initially homogeneous medium with fixed boundary temperatures. They resolved the structure of flame by using an adaptive mesh point method. They obtained the flame speed as a function of the hot side boundary temperature and the cooler side density. Combining the result with the assumption of balanced power between the integrated nuclear energy generation rate and neutrino emission rate, they have concluded that the flame will reach the center if the mass of the white dwarf is greater than $\sim 0.8 M_\odot$. On the other hand, Kawai, Saio, & Nomoto (1987) have shown that carbon burning can ignite in the outer part of an rapidly mass-accreting white dwarf if it is more massive than $1.07 M_\odot$. These results indicate that once carbon-burning is ignited the flame propagates throughout the interior of the white dwarf to convert the C-O mixture into an O-Ne-Mg mixture. Therefore, if the merging of a double white dwarf system leads to an accretion rapid enough to cause an off-center carbon ignition in the primary white dwarf ($\dot{M} \gtrsim 2.7 \times 10^{-6} M_\odot \mathrm{y}^{-1}$; Kawai et al. 1987), no Type Ia supernova is expected. Since it is very important to know what is the final product of the merging of double white dwarfs, we have reinvestigated the flame propagation in a white dwarf by inserting enough grid points to resolve the flame structure.

In a helium white dwarf accreting helium at a rate faster than $2 \times 10^{-8} M_\odot \mathrm{y}^{-1}$ helium burning is ignited off-center (Nomoto & Sugimoto 1977). When we made computations for the massive C-O white dwarf before, we also calculated helium white dwarf models. We found that helium burning shell propagates inward to the center by repeating mild flashes, and that the white dwarf is converted to a helium-main-sequence star. Some of the results have been presented in Nomoto & Hashimoto (1986, 1987). Iben (1990) investigated similar cases and claimed that the products of merging low mass white dwarfs are sdB and sdO stars (see, e.g., Heber (1991) for a review

of sdB and sdO stars). In our present paper we also presents results of additional computations for helium accreting low mass helium white dwarfs.

2. C-O white dwarf

2.1. Structure of flame

In our previous calculation (Saio & Nomoto 1985), the inward propagation of the carbon-burning shell appeared as a series of successive shell flashes. This is an artifact brought by insufficient spatial resolution. The actual evolution should be a nearly steady progression of the burning front or flame (Timmes et al. 1994). In this paper, we present the result of our re-computations for this problem done by inserting enough grid points to resolve the carbon burning flame. Input physics and the initial model are the same as in Saio & Nomoto (1985). Figure 1 shows the flame structure at selected phases when the flame is located at $M_r \simeq 0.6 M_\odot$. The flame, whose center is defined by the peak of nuclear energy generation rate per unit mass $\epsilon_{\rm n}$, moves inward keeping the neighboring structure similar. Just interior to the flame there is a thermal front having an extremely steep temperature gradient. The front moves inward due to the conductive energy flow. Matter experiences a large heating by the passage of the front. The density decreases appreciably between the thermal front and the flame center.

Since the carbon abundance decreases outward in the flame, the maximum temperature occurs at a zone exterior to the flame center. The position of the maximum temperature is recognized in Figure 1 as the point where the direction of energy flow changes (i.e., the sign of L_r changes; dotted lines are used if $L_r < 0$ and long dashed lines if $L_r > 0$ in Fig. 1). Figure 1 indicates that most of the energy produced in the flame flows inward and is used to move the thermal front inward.

Behind the flame (i.e., exterior to the flame) a shell convection zone develops. The bottom of the convection zone is recognized in Figure 1 as sudden decreases of $X_{\rm C}$ and $\epsilon_{\rm n}$. The convection zone at these stages extends to $M_r \simeq 0.73 M_\odot$. A considerable amount of energy is generated from carbon-burning in the convection zone. For the model in the middle panel of Fig. 1, $L_{\rm n} = 7.64 \times 10^6 L_\odot$, in which $4.72 \times 10^6 L_\odot$ is produced in the flame, and the remaining part is produced in the convective zone, and $L_\nu = 3.06 \times 10^6 L_\odot$. Around the outer boundary of the convection zone the outward energy flow is reduced to $L_r \simeq 1.8 \times 10^4 L_\odot$ due to the neutrino emission in the convection zone. Roughly speaking, 40% of the energy generated by carbon burning is lost by neutrino emission and the remaining energy is conducted inward to heat matter between the flame and the thermal front. Nomoto (1984,1987) and García-Berro, Ritossa, & Iben (1997) have obtained similar results for a carbon-burning flame in the asymptotic giant branch phase of a $9 M_\odot$ model.

2.2. Propagation of flame

Keeping grid spacing fine enough to resolve the thermal front and the flame demands very small timesteps to follow the flame propagation. To alleviate the computational effort we used a steady burning approximation occasionally in evolutionary computations. In the steady burning approximation, we do not resolve the structure around the flame; i.e., the thermal front and the flame is represented by a grid point. The total nuclear energy generation rate $L_{\rm n}$ is calculated by

$$L_{\rm n} = X_{\rm C} Q |dm_{\rm f}/dt|, \qquad (1)$$

where Q is the energy yield from carbon burning, for which we have adopted $Q = 4.4 \times 10^{17}$ergs s^{-1}g^{-1}, and $m_{\rm f}$ is the mass coordinate of the flame center. The local energy generation rate per unit mass $\epsilon_{\rm n}$ was set to be zero except at the grid point corresponding to the flame; i.e., $\epsilon_{{\rm n}j} = 0$ if $j \neq J$ and $\epsilon_{{\rm n}J} = L_n/(M_{r,J+1} - m_{\rm f})$, where Jth grid point corresponds to the flame and $M_{r,j}$ represents the mass coordinate at the jth grid point. The value of $\dot{m}_{\rm f}$ for the steady burning calculations was obtained from a few thousand preceding models obtained by usual evolution calculations with fine grid spacings.

In our present investigation, evolutionary calculations were started with a model from Saio & Nomoto (1985). The model has a carbon-burning flame at $m_{\rm f} \sim 0.85 M_\odot$. Interior to the flame, carbon and oxygen abundances are ($X_{\rm C}$,$X_{\rm O}$)=(0.5,0.5). To see the effect of the carbon abundance in the interior, we have also computed a set of evolutionary models starting with the initial model in which the abundance interior to the flame had been artificially converted to ($X_{\rm C}$,$X_{\rm O}$)=(0.2,0.8). In both cases, the accretion rate was kept constant at $10^{-5} M_\odot {\rm y}^{-1}$.

Figures 2 and 3 show evolutionary changes in the nuclear energy generation rate $L_{\rm n}$ (solid line) and the

neutrino energy loss rate L_ν (broken line) as a function of the mass coordinate of the carbon-burning flame $m_{\rm f}$ for $X_C = 0.5$ and 0.2, respectively. In these figures, the phases with constant $L_{\rm n}$ correspond to the evolution phases during which the steady burning approximation was applied. As can be seen from these figures, one set of calculations with the steady burning approximation was stopped when $m_{\rm f}$ changed by $\sim 0.05 M_\odot$. Large fluctuations in $L_{\rm n}$ at the transitions from the steady burning calculation to the normal evolutionary calculation are artificial phenomena caused by inserting grid points just interior to the flame.

In most phase of the progression of the carbon-burning flame the nuclear energy generation rate $L_{\rm n}$ exceeds the neutrino energy loss rate L_ν. As discussed above, the difference is approximately the amount of energy conducted inward. This energy balance is similar to that found by García-Berro et al. (1997) but somewhat different from the balanced power assumption employed by Timmes et al. (1994). For $X_{\rm C} = 0.5$, the inward propagation of the flame stalls at $M_r \sim 0.4 M_\odot$, which appears as a sharp dip of $L_{\rm n}$ in Fig. 2. We discuss this phenomenon more below. In both cases the flame reaches to the center and exhausts carbon interior to the first ignition shell, which confirms our previous conclusion (Saio & Nomoto 1985).

Figures 4 and 5 show the time variation of the distributions of temperature and of density, respectively, during the flame propagation for $X_{\rm C} = 0.5$. The flame temperature is maximum when the burning front is located at $M_r \simeq 0.8 M_\odot$, i.e., when $m_{\rm f} \simeq 0.8 M_\odot$. Then it decreases gradually as the flame propagates toward the center. Since pressure is continuous across the flame, density decreases as matter gets into the flame. The density just interior to the flame is maximum when $m_{\rm f} \simeq 0.9 M_\odot$. It decreases as the flame propagates inward until it becomes minimum when $m_{\rm f} \simeq 0.5 M_\odot$, and then increases slowly as the flame approaches the center. These variations depend on the flame speed, bulk expansion rate of the white dwarf, density gradient, the degree of electron degeneracy, etc.

The central temperature and density decrease as the flame propagates. This variation is caused by the net gain of energy because the nuclear energy generation rate exceeds the neutrino loss rate in most phases of the flame propagation. (When the neutrino loss rate exceeds the nuclear energy generation rate, both the central temperature and density increase [see below].) The decrease of the central temperature seen in Fig. 4 is larger than the case shown in Saio & Nomoto (1985). This can be explained as follows: In Saio & Nomoto (1985), the spatial resolution was not enough so that the flame propagation appeared as a series of shell-flash and inter shell-flash phases. During an inter shell-flash phase, the neutrino loss rate exceeded the nuclear energy generation rate. Therefore, the net gain of energy in the present calculation is higher than the case in Saio & Nomoto (1985).

The time variation of $m_{\rm f}$ for $X_{\rm C} = 0.5$ is shown in Figure 6 by the dashed line. The solid line and the dotted line in this figure show the position of thermal front for $X_{\rm C} = 0.5$ and 0.2, respectively. The shell having $\log T = 7.7$ well represents the position of the thermal front, which is located just interior to the flame (see Fig. 1). The propagation speed of the flame for $X_{\rm C} = 0.5$ decreases significantly and the flame stalls for a while at $M_r \sim 0.4 M_\odot$. This phase corresponds to a deep dip in $L_{\rm n}$ seen in Fig. 2. Even when the flame propagation stops, the thermal front gradually moves inward but the steepness of the temperature gradient decreases (Fig. 7 below). After the flame have stalled there for ~ 4000 years, it becomes active again and propagates toward the center at a speed considerably slower than before. After the reactivation, the carbon abundance in the convective shell is ~ 0.1, which is considerably higher than the case before the flame stalled. After the flame reached the center, the remaining carbon has been burnt quietly in a few thousand years.

The flame for $X_{\rm C} = 0.2$, on the other hand, reaches the center smoothly in ~ 1000 years and the thermal front keeps very close to the flame during the propagation. Since the flame remains strong throughout the propagation in this case, the carbon abundance in the convective zone never exceed 0.005. Therefore, when the flame reached the center, most of carbon in the region interior to the first ignition shell has been exhausted.

Figures 7 and 8 show variations of temperature and density distributions, respectively, in the phase during which the propagation of the flame almost stopped and was re-activated later for $X_{\rm C} = 0.5$. Upper and lower panels of these figures show evolution before and after the re-activation of flame, respectively. The direction of evolution is recognized by the inward propagation of the thermal front. The last lines in the upper panels are the same phase as the first lines in

the lower panels. Before the re-activation, as the thermal front propagates inward, the temperature gradient at the front becomes less steep and the density jump gets smaller and less apparent. During this phase, the flame becomes weak and hardly moves at $M_r \simeq 0.42 M_\odot$ (Fig. 6). Since $L_{\rm n} < L_\nu$ in the phases shown in the upper panels of these figures, the density interior to the front increases with time. The burning becomes active again at $M_r \sim 0.4 M_\odot$, when the thermal front is located around $M_r \sim 0.35 M_\odot$. A new thermal front backed by the activated flame appears outside of the old front and propagates inward to engulf the old one at $M_r \simeq 0.345 M_\odot$.

The time spent for the flame to reach the center is shorter for $X_{\rm C} = 0.2$ than the case of $X_{\rm C} = 0.5$. Moreover, for $X_{\rm C} = 0.5$ the flame in the present calculation takes longer to reach the center than in our previous calculation (Saio & Nomoto 1985), in which it took about 5000 years for the flame to propagate through the interior. Such differences can be explained by the fact that the net-energy gain $(L_{\rm n} - L_\nu)$ in the present $X_{\rm C} = 0.5$ case is larger than the $X_{\rm C} = 0.2$ case or our previous calculation. A larger energy-gain makes gentle the temperature increase in the inner part of the flame, because a larger energy-gain decreases more the density at the ignition temperature, thus making the degree of degeneracy there lower. A lower temperature gradient makes the propagation speed lower.

2.3. Discussion

Timmes et al. (1994) evaluated propagation speeds of carbon-burning flames in a isobaric region which has initially homogeneous temperature and density. They obtained flame speed in such systems as a function of the boundary temperature of the hotter side and the density of the cooler side (initial density) of the flame. The boundary temperature in the cooler side (i.e., initial temperature) was fixed at 5×10^8K, which is much higher than in our models. Figure 9 shows the propagation speed $|dm_{\rm f}/dt|$ of the flame derived from the actual propagation in our evolutionary models for $X_{\rm C} = 0.2$ (filled circles) and that taken from the table of propagation speed for $X_C = 0.2$ in Timmes et al. (1994) for the density and temperature at the flame in our models (open circles). This figure indicates that the propagation speed based on Timmes et al.'s result tends to be higher than that in our evolutionary models. One reason for this difference may be ascribed to the fact that the cooler side temperature of our models is much lower than that in Timmes et al.'s analyses. We note here that evolution calculations using the steady state approximation with the propagation speed of Timmes et al. failed before the flame reaches the center because the density became too low. The rapid density decrease occurred because the energy production rate was too high, which indicates that their propagation speed seems too high for our white dwarf models.

We have found a new phenomenon that the propagation of the flame tends to be oscillatory when the peak temperature is relatively high. An example is shown in Figs. 10 and 11. The lower panel of Fig. 10 shows runs of temperature in the interior for every 20 evolutionary models, while the upper panel shows nuclear energy generation rate $L_{\rm n}$ and neutrino emission rate L_ν as functions of $m_{\rm f}$ (time advances from right to left of the diagram). Figure 11 shows $L_{\rm n}$ and L_ν as functions of time. As seen in Fig 10, the temperature gradient between the ignition point ($\log T \simeq 8.8$) and the position of maximum temperature becomes gentle occasionally, and the energy generation rate dips. The time variation of L_n is characterized by semi-regular oscillations with sharp peaks and relatively gentle minimums. The typical 'period' is an order of 0.1y. In contrast to the variation of L_n, L_ν hardly changes.

Such oscillatory behavior of the flame tends to occur when the thermal front is resolved by finer grid spacings. Since finer grid spacings make the maximum temperature steepness of the thermal front larger, we infer that a steep temperature gradient plays an important role in the instability. We may explain the cause of the fluctuation as follows: When the temperature gradient becomes too steep, the inward energy flow exceeds the energy generation by nuclear burning to decrease the flame temperature and hence L_n. This decreases the steepness of temperature distribution, which in turn slows the inward energy flow. Then, the flame temperature and L_n increase to recover the previous levels.

It is known that a combustion flame front in a solid medium (in which the diffusion rate of the fuel is much slower than the rate of thermal conduction) is thermally unstable if the temperature sensitivity of the energy generation rate is sufficiently high (see e.g., Zeldovich et al 1985). The high temperature sensitivity of energy generation rate makes the flame thin with a steep temperature gradient. We believe that the instability is the same as that of the carbon-

burning flame in our accreting white dwarf because both of them occur under the condition of a steep temperature gradient and a high temperature sensitivity of energy generation rate.

3. Heium white dwarf

The starting model adopted for a helium-accreting white dwarf is a chemically homogeneous (Y=0.98, Z=0.02) white dwarf of $0.4M_\odot$. The white dwarf is assumed to be the massive component of a double white dwarf system. When the less massive component fills the critical Roche lobe (because of the gravitational wave radiation), the mass transfer is unstable if the mass ratio exceeds 2/3. In this case the massive component is expected to accrete matter at a rate of the Eddington limit, which is of the order of $10^{-5}M_\odot\mathrm{yr}^{-1}$. If the mass ratio is less than 2/3, stable mass transfer occurs at a rate of e.g., $3\times10^{-6}\mathrm{yr}^{-1}$ for $M_2=0.2M_\odot$, and $5\times10^{-8}M_\odot\mathrm{yr}^{-1}$ for $M_2=0.1M_\odot$, where M_2 indicates the mass of the less massive component. Iben (1990) investigated the consequences of rapid merger processes in which mass is accreted at a rate faster than the critical Eddington limit. We investigate here cases with mass accretion rates $10^{-7}M_\odot\mathrm{yr}^{-1}$ and $10^{-6}M_\odot\mathrm{yr}^{-1}$, which are much smaller than the critical Eddington limit.

The chemical composition of accreting matter is set to be (Y,Z)=(0.98,0.02) assuming that the less massive component is also a helium white dwarf.

3.1. Results

Accretion causes heating in the envelope of the white dwarf. When a sufficient mass is accreted, the triple alpha reaction is ignited. For higher accretion rate the total mass at the helium ignition is lower and the mass between the ignition shell and the surface is smaller. The ignition occurs at $M_r\simeq0.44M_\odot$ when the total mass becomes $M\simeq0.52M_\odot$ for $\dot{M}=10^{-7}M_\odot\mathrm{y}^{-1}$; these quantities are, respectively, $M_r\simeq0.41M_\odot$ and $M\simeq0.45M_\odot$ for $\dot{M}=10^{-6}M_\odot\mathrm{y}^{-1}$. The ignition of the triple alpha reaction leads to a shell flash (thermal pulse).

After the shell flash is over, another shell flash occurs at a slightly inner shell than the previous one. Such shell flashes repeat $\sim$ 20 to 30 times until the ignition shell reaches the center of the star. The number of shell flashes is larger than for the cases investigated by Iben (1990). The difference is attributed to the fact that the first ignition shell in Iben's models ($M_r\sim0.25M_\odot$) is closer to the center than our models. Figure 12 shows the time variation of the integrated nuclear energy generation rate L_n in solar units for $\dot{M}=10^{-6}M_\odot\mathrm{y}^{-1}$. The strength of a shell flash decreases as the ignition shell moves inward. The evolution of repeating mild flashes is similar to the evolution which occurs after the ignition of helium core flash in a red giant star (e.g., Mengel & Sweigart 1981).

The first shell flash is stronger for the lower accretion rate, because the density at the ignition shell is higher. At the peak of the first shell flash $\log L_\mathrm{n}$ reaches up to $\sim$ 7.5 for $\dot{M}=10^{-6}M_\odot\mathrm{y}^{-1}$, while $\sim$ 10.3 for $\dot{M}=10^{-7}M_\odot\mathrm{y}^{-1}$. The strength of the second and the later shell flashes hardly depends on the accretion rate.

Figure 13 shows the time variation of the mass coordinate m_f where the nuclear energy generation rate per unit mass is maximum. The zero point of time in this figure is set at the first ignition of helium burning. The helium burning shell reaches the center in $\sim5.7\times10^5$y for $\dot{M}=10^{-6}M_\odot\mathrm{y}^{-1}$ and in $\sim1.2\times10^6$y for $\dot{M}=10^{-7}M_\odot\mathrm{y}^{-1}$ after ignition. The inward move of m_f is faster for higher accretion rate because the total mass is larger. The total mass increases to about $1M_\odot$ before the burning shell reaches the center for $\dot{M}=10^{-6}M_\odot\mathrm{y}^{-1}$, while $0.63M_\odot$ for $\dot{M}=10^{-7}M_\odot\mathrm{y}^{-1}$. At each shell flashes, a convection zone appears above the burning shell. One shell flash ends when the helium abundance in the convection zone decreases to $\sim$ 0.90. Therefore, when the burning shell reaches the center, the star becomes to have a structure similar to that of the zero-age helium main-sequence.

The inward propagation of the burning shell does not stop even if the accretion stops. Figure 13 includes two cases in which accretion has stopped before the burning shell reaches the center. In one case, A6S45, the accretion ($\dot{M}=10^{-6}M_\odot\mathrm{y}^{-1}$) has stopped when the total mass became $0.45M_\odot$ (just after the first shell flash) and in another case, A6S50, the accretion has stopped when the total mass became $0.5M_\odot$ (when the burning shell was located at $M_r\simeq0.3M_\odot$). The time in which helium burning reaches the center for A6S45 is about 2.7×10^6, which is longer than for A6S50 and is similar to Iben's (1990) $0.46M_\odot$ case. Since the accretion process assumed in Iben (1990) is quite different from ours, we can conclude that the time is mainly determined by the total mass and is insensitive to the accretion rate itself.

Figure 14 shows the evolutionary paths of our accreting helium white dwarfs in the HR diagram. After accretion starts the luminosity increases along the white dwarf sequence until the triple-alpha reaction is ignited. Once the ignition occurs, the luminosity decreases at first and increases later. By the end of the first shell flash, the star moves into the super-giant region. From this behavior we can infer that even if the mass transfer is stable and $\dot{M}$ is as low as $1 \times 10^{-7} M_\odot \mathrm{y}^{-1}$, once helium burning is ignited, the radius increases to engulf the companion. As the burning shell moves inward with repeating shell flashes, the star gradually evolves blueward to the helium-main-sequence. The redward extension of the evolutionary paths during the phase of repeating flashes is larger than Iben's (1990) models, because in the latter models the mass above the first ignition shell ($> 0.1 M_\odot$) is larger than in our models ($\sim 0.04 M_\odot$ for $\dot{M} = 1 \times 10^{-6}$, and $\sim 0.07 M_\odot$ for $\dot{M} = 1 \times 10^{-7}$).

When the burning shell reached the center, the accretion rate was set to be zero. Then, the total mass is $0.63 M_\odot$ for $\dot{M} = 1 \times 10^{-7}$ and $1.01 M_\odot$ for $\dot{M} = 1 \times 10^{-6}$. After the burning shell has reached the center, the star spends core helium burning phase as a helium-main-sequence star which lasts of order of 10^7y. The star evolves off the helium main-sequence when the helium is exhausted in the core. The star with $0.63 M_\odot$ (dotted line) evolves to become brighter and bluer and will evolve along with the white dwarf cooling sequence. The star with $1.01 M_\odot$ evolves to super-giant region again; the behavior is known from the helium star evolution calculations by e.g., Paczyński (1971) and Saio (1995).

3.2. Discussion

3.2.1. Comparison with the case of carbon-oxygen white dwarfs

Figure 15 shows runs of the temperature and the rate of gravitational energy release $\epsilon_{\rm g}$ around the burning shell at selected stages from the peak of a shell flash to the next one. The number for each curve indicates the corresponding model number. At the peak of a shell flash a sharp peak appears in the temperature distribution (#951 and #1251), and a zone exterior to the temperature peak has negative $\epsilon_{\rm g}$, which indicates that it is expanded by absorbing heat released by the helium burning. This figure also shows that during the inter-flash period, the layer beneath the flashed shell is heated by compression (i.e., $\epsilon_{\rm g} > 0$). The next shell flash occurs at a shell in the heated layer. Thus, the main driving force of the inward propagation of the burning shell is the compressional heating during the inter-flash phase. This differs from the case of the carbon burning flame. In the latter case, as discussed in the previous section, inward conductive heat flow is the main cause for the flame propagation.

In the case of carbon burning flame the burning shell exhausts carbon during the inward propagation and most of the released nuclear energy is conducted inward or lost by neutrino emission in the convection zone just above the flame. In the case of helium burning shell, on the other hand, only a small fraction of helium is converted to carbon and oxygen during the inward progression of the burning shell and neutrino emission rate is always much smaller than the nuclear energy release.

3.2.2. Relation with observed double white dwarf systems

Several double white dwarf systems which consist of low mass ($\lesssim 0.4 M_\odot$) white dwarfs have been found (Saffer, Liebert, & Olszewski 1988, Bragaglia, Greggio, & Renzini 1990, Marsh, Dillon, & Duck 1995, Marsh 1995). The secondary components of these systems seem to have comparable masses. Since the masses of those white dwarfs are too small to ignite the triple alpha reaction by the effect of their own gravity, these are probably helium white dwarfs. Although all the systems are detached, some of the systems have orbital periods of a few hours and are expected to become semi-detached systems in a few billion years (Marsh et al. 1995, Marsh 1995).

When the less massive component of a double white dwarf system exceeds its critical Roche lobe, mass transfer starts. If the mass ratio of the secondary to the primary is higher than about 2/3, mass transfer on the dynamical time scale is expected to occur (at least in the beginning) to form a common envelope, and the primary accretes matter at a rate of the critical Eddington limit. Even if the mass ratio is smaller and mass transfer is stable, a common envelope is expected to be formed because the radius of the primary becomes the supergiant size after the triple alpha reaction is ignited in the primary as discussed above (Fig. 14).

We do not know exactly what is the consequence

of the common envelope phase. We infer that matter is peeled off from the secondary. If the system loses angular momentum effectively enough, the separation between the primary and the secondary decreases to merge (i.e., 'spiral-in' occurs). The system would become a single helium star with a mass of $\lesssim 0.8M_\odot$, which will eventually become a DB white dwarf.

If the systemic loss of angular momentum is not large, the separation can increase as the mass transfer proceeds. In this case, common envelope phase ends when the radius of the primary shrinks and the remnant of the secondary gets out of the primary envelope. Considering the fact that there exist recurrent novae, in which in each nova explosion the secondary component is engulfed in the expanding envelope, we infer that the secondary in the double white dwarf system can survive the common envelope phase. In the double white dwarf system, however, the separation is much smaller and the duration of the common envelope phase is much longer than in the case of novae. Therefore, it is expected that a significant amount of mass is peeled off from the secondary. If the secondary survives, the remaining system would have a primary in the helium main sequence phase with a mass less than $0.8M_\odot$ and a secondary white dwarf having a very small mass. After helium is exhausted in the primary, the system becomes a double white dwarf system with a small mass ratio. Such a system loses its angular momentum by the gravitational wave emission and eventually the less massive component fills its critical Roche lobe to resume mass transfer. (Because of the small mass ratio, the mass transfer is dynamically stable.) Such interacting double white dwarf systems can be identified as AM CVn type stars, which are hydrogen-deficient cataclysmic variables composed of double white dwarfs with a small mass ratio ($M_2/M_1 < 0.1$; see Warner (1995) for a thorough review on the AM CVn stars).

4. Conclusion

We have investigated the consequences of merging double white dwarf systems by calculating evolutionary models for accreting white dwarfs. We have considered two cases; a massive C-O white dwarf of $\sim M_\odot$ accreting C-O mixture, and a low mass white dwarf with a initial mass of $0.4M_\odot$.

For the C-O white dwarf an accretion rate of $1\times10^{-5}M_\odot\mathrm{y}^{-1}$ was assumed. After the carbon burning is ignited at $M_r \sim 1.04M_\odot$, the flame propagates inward due to heat conduction. We have considered two extreme cases for the interior abundance of the massive white dwarf: $X_\mathrm{C} = 0.5$ and $X_\mathrm{C} = 0.2$. For $X_\mathrm{C} = 0.5$, the flame becomes very weak at $M_r \sim 0.4M_\odot$ and the inward propagation stalls there. But a few thousand years later, the flame is reactivated due to contraction and propagates to the center. For $X_\mathrm{C} = 0.2$, the flame propagates smoothly and reaches the center in ~ 1000 years. In both cases, most of the interior of the white dwarf has been converted from the C-O mixture into an O-Ne-Mg mixture without causing an explosive phenomenon. Therefore, if the merging of a double C-O white dwarf system leads to an accretion onto the primary white dwarf rapid enough to ignite carbon off-center, we cannot expect a Type Ia supernova but the formation of a neutron star (Saio & Nomoto 1985; Nomoto & Kondo 1991). We have found a new phenomenon that the flame propagation tends to be oscillatory when the peak temperature is relatively high.

For the helium white dwarf we have considered accretion rates $10^{-7}M_\odot\mathrm{y}^{-1}$ and $10^{-6}M_\odot\mathrm{y}^{-1}$. In each case, when a certain amount of helium is accreted, the triple-alpha reaction is ignited in the outer part and a shell flash (thermal pulse) occurs. The helium burning shell moves inward by repeating alternatively shell flashes and inter-flash compression. The burning shell reaches the center on a timescale of order 10^6y after the first ignition. The inward progression does not stop even if the accretion has stopped after the first shell flash. At each shell flash a convection zone is formed. When the helium abundance in the convective layer decreases by $\sim 10\%$, the shell flash diminishes. When the burning shell reached the center the star has a structure similar to that of zero-age helium main-sequence star. Such a star is expected to evolve as a helium star to finally become a DB white dwarf. We have also discussed the possibility that a low mass double white dwarf system could be a progenitor of the AM CVn stars.

This work has been supported in part by the grant-in-Aid for Scientific Research (05242102, 06233101, 7223202) and COE research (07CE2002) of the Ministry of Education, Science, and Culture in Japan. KN's research at the Institute for Theoretical Physics has been supported in part by the National Sceince Foundation in US under Grant No. PHY94-07194.

REFERENCES

Benz, W., Bowers, R.L., Cameron, A.G.W., & Press, W.H. 1990, ApJ, 348, 647

Bragaglia, A., Greggio, L., Renzini, A., & D'Odorico, S. 1990, ApJ, 365, L13

Bragaglia, A. 1995, in White Dwarfs, eds. D.Koester & K.Werner, Lect. Not. Phys. 443 (Berlin: Springer), 238

Cameron, A.G.W., Iben, I. 1986, ApJ, 305, 228

Foss, D., Wade, R.A., & Green, R.F. 1991, ApJ, 374, 281

García-Berro, E., Ritossa, C., Iben, I.Jr. 1997, ApJ, 485, 765

Hachisu, I., Eriguchi, Y., & Nomoto, K. 1986, ApJ, 308, 161

Heber, U. 1991, in Evolution of Stars: The Photospheric Abundance Connection, eds. G.Michaud and A.Tutukov, IAU Symp. 145 (Dordrecht: Reidel), 363

Iben, I.Jr. 1990, ApJ, 353, 215

Iben, I.Jr., & Tutukov, A. 1984, ApJS, 55, 335

Kawai, Y., Saio, H., & Nomoto, K. 1987, ApJ, 315, 229

Marsh, T.R. 1995, MNRAS, 275, L1

Marsh, T.R., Dhillon, V.S., & Duck, S.R. 1995, MNRAS, 275, 828

Mengel, J.G. & Swigart, A.V. 1981, in Astrophysical Parameters for Globular Clusters, ed. A.G.D. Philip (Dordrecht: Reidel), 277

Mochkovitch, R., & Livio, M. 1990, A&A, 236, 378

Nather, R.E., Robinson, E.L., & Stover, R.J. 1981, ApJ, 244, 269

Nomoto, K. 1984, ApJ, 277, 791

Nomoto, K. 1987, ApJ, 322, 206

Nomoto, K., & Hashimoto, M. 1986, Prog. Nucl. Phys. 17, 267

Nomoto, K., & Hashimoto, M. 1987, Ap&SS, 131, 395

Nomoto, K., & Iben, I.Jr. 1985, ApJ, 297, 351

Nomoto, K., & Kondo, Y. 1991, ApJ, 367, L19

Nomoto, K., & Sugimoto, D. 1977, PASJ, 29, 765

Saffer, R.A., Liebert, J., & Olszewski, E.W. 1988, ApJ, 334, 947

Saio, H. 1995, MNRAS, 277, 1393

Saio, H., & Nomoto, K. 1985, A&A, 150, L21

Paczyński, B. 1971, *Acta Astr*, 21, 1

Robinson, E.L., & Shafter, A.W. 1987, ApJ, 332, 296

Timmes, F.X., Woosley, S.E., & Taam, R.E. 1994, ApJ, 420, 348

Warner, B. 1995, Ap&SS, 225, 249

Webbink, R.F. 1984, ApJ, 277, 355

Woosley, S.E., & Weaver, T.A. 1986, in Nucleosynthesis and Its Implications for Particle Physics, ed. J. Audouze & T.van Thuan (Dordrecht: Reidel), 145

Zeldovich, Ya.B., Barenblatt, G.I., Librovich, V.B., Makhviladze, G.M. 1985, The Mathematical Theory of Combustion and Explosions (New York: Consultants Bureau)

This 2-column preprint was prepared with the AAS LaTeX macros v4.0.

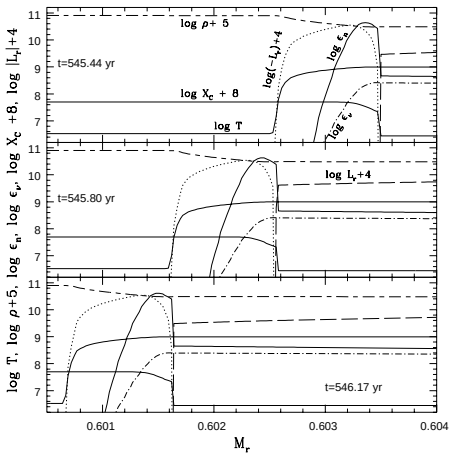

Fig. 1.— Runs of density ρ, temperature T, carbon abundance X_C, nuclear energy generation rate per unit mass $\epsilon_{\rm n}$, neutrino emission rate per unit mass ϵ_ν, and L_r around the carbon-burning flame at selected stages of the flame propagation. To display the variation of L_r, the dotted lines are used when $L_r < 0$ and the long dashed-lines when $L_r > 0$.

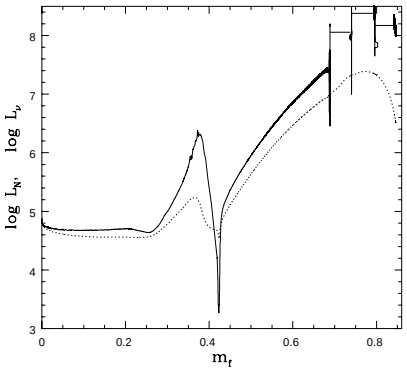

Fig. 2.— Total nuclear energy generation rate $L_{\rm n}$ (solid line) and neutrino energy loss rate L_ν (dotted line) are shown as functions of $m_{\rm f}$ (the mass coordinate at the carbon burning flame) for $X_C = 0.5$. The phases with constant $L_{\rm n}$ correspond to the phases during which the steady burning approximation was applied. Large fluctuations in $L_{\rm n}$ at the ends of such phases are artifacts caused by inserting many grid points around the flame.

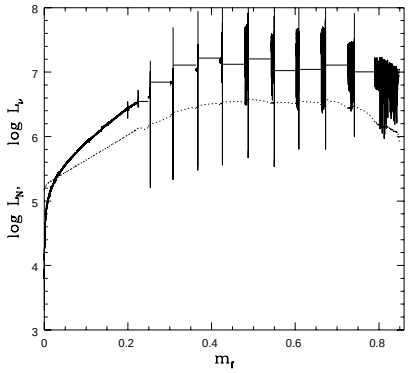

Fig. 3.— The same as Fig. 2 but for $X_{\rm C} = 0.2$

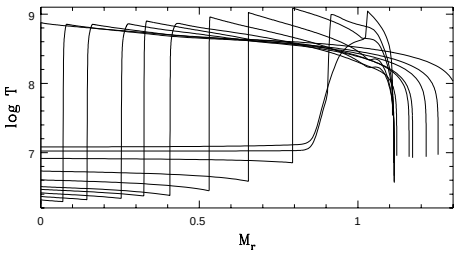

Fig. 4.— Variation of the temperature distribution as the carbon-burning flame propagates inward.

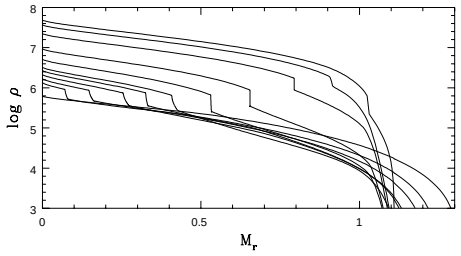

Fig. 5.— Variation of the density distribution as the carbon-burning flame propagates inward.

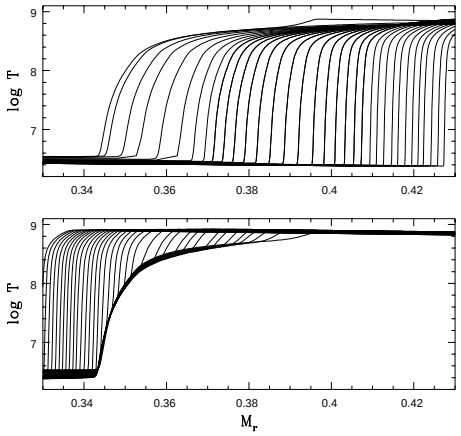

Fig. 7.— Evolution of temperature distribution before (upper panel) and after (lower panel) the re-activation of flame.

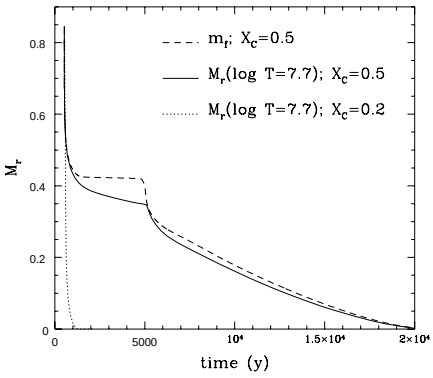

Fig. 6.— Changes in the position of flame (dashed line) and thermal front (solid line) for $X_{\rm C} = 0.5$. The dotted line indicates the thermal front for $X_{\rm C} = 0.2$, for which the flame is always very close to the thermal front.

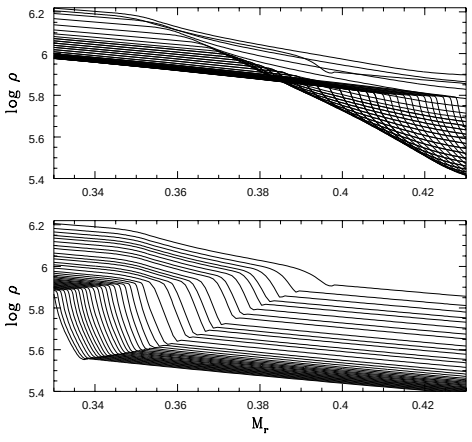

Fig. 8.— Evolution of density distribution before (upper panel) and after (lower panel) the re-activation of flame.

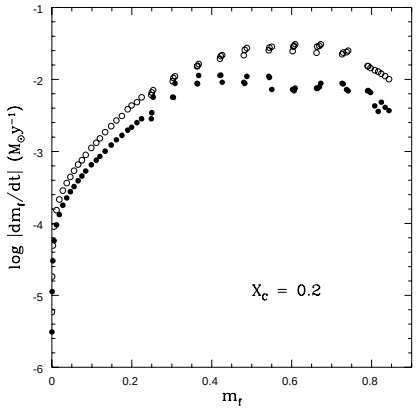

Fig. 9.— Propagation speed $|dm_{\rm f}/dt|$ $(M_\odot {\rm y}^{-1})$ versus position $m_{\rm f}$ of the flame for $X_{\rm C} = 0.2$. Filled circles represent propagation speed evaluated from the propagation of the flame in evolutionary models, while open circles represent the values obtained by interpolating Timmes et al.'s (1994) table for the density and temperature at the flame.

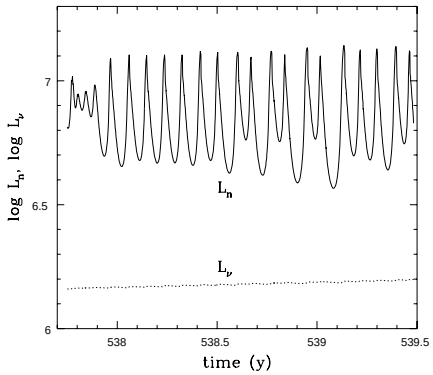

Fig. 11.— The time variations of $L_{\rm n}$ and L_ν during the evolution phase shown in Fig. 10.

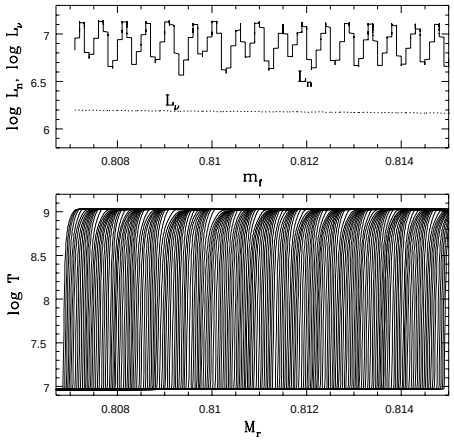

Fig. 10.— The upper panel shows $L_{\rm n}$ and L_ν as functions of the mass coordinate of the flame for $X_{\rm C} = 0.2$. Time runs from right to left. The lower panel shows temperature distribution near flames at various evolutionary stages.

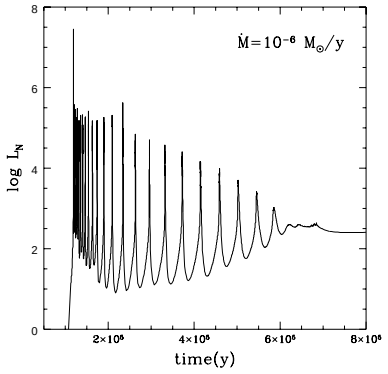

Fig. 12.— The time variation of the integrated nuclear energy generation rate during the process of inward propagation of the helium burning shell for $\dot{M} = 10^{-6} M_\odot {\rm y}^{-1}$.

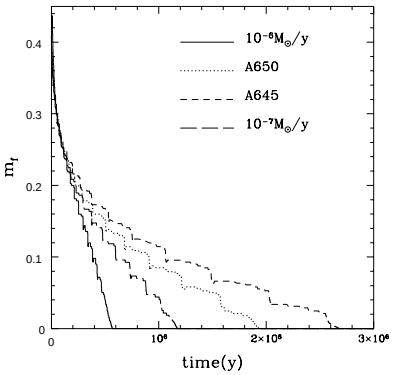

Fig. 13.— The mass coordinate at the helium burning shell versus time after the ignition.

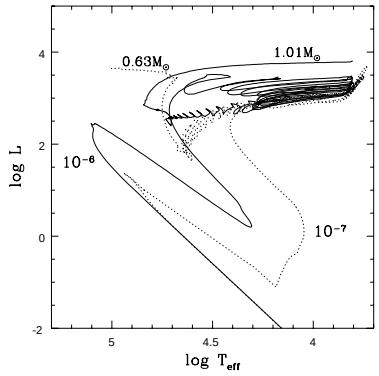

Fig. 14.— The HR diagram showing evolutionary paths of accreting white dwarfs with $\dot{M} = 1.0 \times 10^{-6} M_\odot \mathrm{y}^{-1}$ (solid line) and $\dot{M} = 1.0 \times 10^{-7} M_\odot \mathrm{y}^{-1}$ (dotted line). (The accretion is terminated when the burning shell reaches the center.)

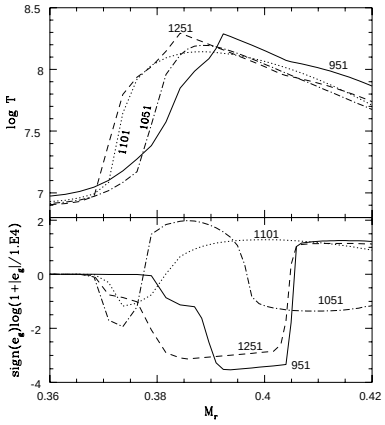

Fig. 15.— Runs of temperature (upper panel) and the rate of gravitational energy release (ϵ_g, lower panel) around the temperature maximum at some selected stages during one cycle of a shell flash (from a peak of shell burning to the next one).